

TOWARDS THERMAL SIMULATION OF POWDER BED FUSION ON PATH LEVEL

Yaqi Zhang

Spatial Automation Laboratory
University of Wisconsin - Madison
Madison, WI 53706

Vadim Shapiro*

Spatial Automation Laboratory
University of Wisconsin - Madison
Madison, WI 53706

Paul Witherell

Engineering Laboratory
National Institute of Standards and Technology
Gaithersburg, MD 20899

ABSTRACT

Powder bed fusion (PBF) is a widely used additive manufacturing (AM) technology to produce metallic parts. Understanding the relationships between process parameter settings and the quality of finished parts remains a critical research question. Developing this understating involves an intermediate step: Process parameters, such as laser power and scan speed, influence the ongoing process characteristics, which then affect the final quality of the finished parts. Conventional approaches to addressing those challenges such as powder-based simulations (e.g., DEM) and voxel-based simulations (e.g., FEM) can provide valuable insight into process physics. Those types of simulations, however, are not well-suited to handle realistic manufacturing plans due to their high computational complexity.

Thermal simulations of the PBF process have the potential to implement that intermediate step. Developing accurate thermal simulations, however, is difficult due the physical and geometric complexities of the manufacturing process. We propose a new, meso-scale, thermal-simulation, which is built on the path-level interactions described by a typical process plan. Since our model is rooted in manufactured geometry, it has the ability to produce scalable, thermal simulations for evaluating realistic process plans. The proof-of-concept simulation result is validated against experimental results in the literature and experimental results from National Institute of Standards and Technology (NIST).

In our model, the laser-scan path is discretized into elements, and each element represents the newly melted material.

An element-growth mechanism is introduced to simulate the evolution of the melt pool and its thermal characteristics during the manufacturing process. The proposed simulation reduces computational demands by attempting to capture the most important thermal effects developed during the manufacturing process. Those effects include laser-energy absorption, thermal interaction between adjacent elements and elements within the underneath substrate, thermal convection and radiation, and powder melting.

1 Introduction

1.1 Motivation

Additive Manufacturing (AM) processes allow for the production of fully functional parts with sophisticated geometries directly from raw materials (e.g., metal powders), complementing traditional manufacturing processes such as subtractive processes and formative processes [1]. In the last few years, there has been a significant industrial increase in the use of metal AM processes to fabricate structural, load-bearing parts. The reason is simple: metal AM allows industry to take advantage of the inherent design freedoms and significant weight savings [2]. One of the most commonly used metal AM processes is the powder bed fusion (PBF) process [3].

*Address all correspondence to this author.

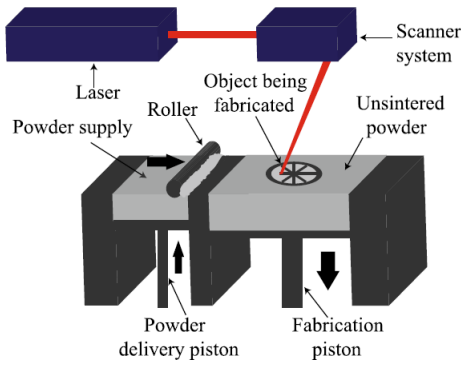


FIGURE 1: Schematic of a typical PBF set-up [4].

During the PBF manufacturing process (see Figure 1), a laser (or electron beam) locally melts and consolidates metal powders along a predefined tool path. Upon completion of each layer, additional powder is spread onto the bed from an adjacent reservoir and evenly distributed by a roller or a blade. This process continues until the whole part is finished (or the build fails). The physics associated with the PBF process, however, creates inherent variabilities in the structure of the manufactured part. Those variabilities arise because of the constant cooling and heating, which creates challenges in fabricating fully dense parts. Pores and stresses are often created, and cracking may result.

To mitigate the heating and cooling effects of the laser, PBF machine manufacturers offer suites of scan patterns from which a machine operator can choose. Today, common practice is that scan patterns are agnostic to the geometry of the part being fabricated. We postulate the opposite is desired. Scan-pattern choice directly influences the geometry of the both melt pool and the final part. Consequently, we propose that an optimal, customized scan pattern will improve control over exposure times, melt-pool sizes, and temperature gradients. These improvements will reduce the defects that occur because of part exposure to the cyclic, thermal cycles that occur during fabrication.

To find this optimal scan pattern, our approach uses computationally efficient thermal simulations to predict thermal histories during part fabrication. These simulations use melt pool characteristics to iterate through potential manufacturing plans for a given part geometry. The simulation results provide decision criteria for selecting the best-fit scan pattern. In this paper, we concentrate on the modeling and simulation of the melt pool at the path level.

PBF uses either a laser or an electron beam as a moving heat source to melt, fuse, and solidify material powder into desired geometries. The initial state of material is uniform loose powder. During the manufacturing process, laser heat provokes coalescence of powder particles causing phase changes from solid to liquid, and possibly even to gas. The temperature field evolution

has significant effects on that coalescence, which, in turn, impacts the properties of the fabricated components. Those properties include density, dimensions, mechanical properties and microstructure. [5]. Uneven temperature gradients, caused by the moving heat source, impacts those properties negatively and may lead to accumulated residual stress, which often results in build failures such as warping, voids in solid material, or the delamination of layers [6, 7].

Clearly, PBF is an inherently complex process. We propose the use of thermal simulations to enable a better understanding of the impacts of PBFs physical phenomena on the final part properties. Thermal simulation acts as the critical tool to build mappings from manufacturing parameters (e.g., laser power, scan speed) to the part properties and optimize manufacturing parameters. These mappings provide a path to optimized manufacturing parameters.

Thermal simulation of PBF is challenging due to the physical and geometric complexity of the manufacturing process as well as its inherent computational complexity, which requires numerical solution at every time increment of the process. Simplifications in simulating the process may provide a means to reduce the latter challenge. A commonly used simplification relies on voxelization of the design geometry followed by solving the transient problem numerically (e.g., finite element analysis). Voxelization approaches, however, do not account for the discrepancy between design (and melt pool) geometry and as-manufactured geometry; hence, they are not as well suited for process plan optimization. Another common simplification approach uses the discrete element method (DEM) to model powder particles as discrete spheres, simulating the thermal and mechanical interactions of those spheres [4]. DEM approaches are usually extremely computationally expensive because they conduct simulations in very short temporal scales and small spatial scales. Neither approach described is suitable for simulating realistic manufacturing plans for parts with complex geometries.

1.2 Approach and contribution

We propose a new path-level thermal simulation of the PBF process. As a meso-scale model, the proposed thermal simulation has the advantage of efficiency over the traditional voxel-based and powder-based methods. Moreover, meso-scale characteristics provide the scalability to simulate realistic manufacturing plans with complicated geometries. The computing domain of the underlying thermal model is generated by discretizing the laser scan path into elements. Each element represents the newly added volume caused by sweeping the melt pool in a short period of time. An element growth mechanism is also introduced to simulate the evolution of melt pool during the manufacturing process. The element-based simulation captures the essential physics during the manufacturing process, including: laser energy absorption, the thermal interactions between adjacent el-

ements (including the adjacent powder and material underneath the substrate), the thermal convection and radiation, and the melting of the metal powder.

Due to the computational complexity of simulating the entire PBF process, we first focus on simulating a single path of the laser beam scanning over a thin layer of metallic powder placed on a dense substrate of the same material. The resulting path-level simulation assumes that a single track can be accurately modeled with a union of interacting discrete elements, where each element is formed by solidification of the moving melt pool. These single-track, proof-of-concept simulations allow for the experimental validation of our approach, focusing on the characterization of the melt pool, melt-pool geometry, and melt-pool-thermal dynamics while avoiding additional complexities.

To demonstrate and validate the proposed simulation, we applied the approach to simulate PBF processes with two different materials (316L stainless steel and Inconel Alloy 625) and compare the simulation results with both experimental data and high-fidelity simulations results. We found that our simulation result agrees very well with both the experimental data and high-fidelity simulation results. As such, the work reported here provides early results for a simulation that will become increasingly complex as additional geometries are integrated, providing a foundation on which additional capabilities can be built. An example of the discretization of a single layer [8] part is shown in Fig. 2, where the blue line denotes the path plan of the laser scan and the red dots denote the centers of elements.

The remainder of this paper is organized as follows: Related work is briefly discussed in Section 2. The main contributions of the paper are contained in Section 3. Problem formulation and numerical schemes are introduced in Section 3.1. Sections 3.2 and 3.3 describe laser modeling and how to model material properties. An element growth mechanism is introduced in Section 3.4. Section 3.5 summarizes the whole simulation. Section 4 describes two numerical experiments to validate the proposed simulation. Finally, Section 5 is devoted to the conclusion and discussion of future work.

2 Related work

Thermal field evolution has significant influence on both geometric and mechanical properties of the final fabricated components. Therefore, many researchers have focused their efforts on understanding the physical phenomena developed in PBF process and have proposed models to describe the thermal evolution [9–12]. Dai et al. [13, 14] studied the thermal field of dental porcelain using PBF. Matsumoto et al. [15] applied finite element methods to study the distribution of temperature and stress of single layer forming of PBF. Dong et al. [16] and Kolossov et al. [17] created three-dimensional finite element (FE) models studying the temperature evolution during laser melting, with

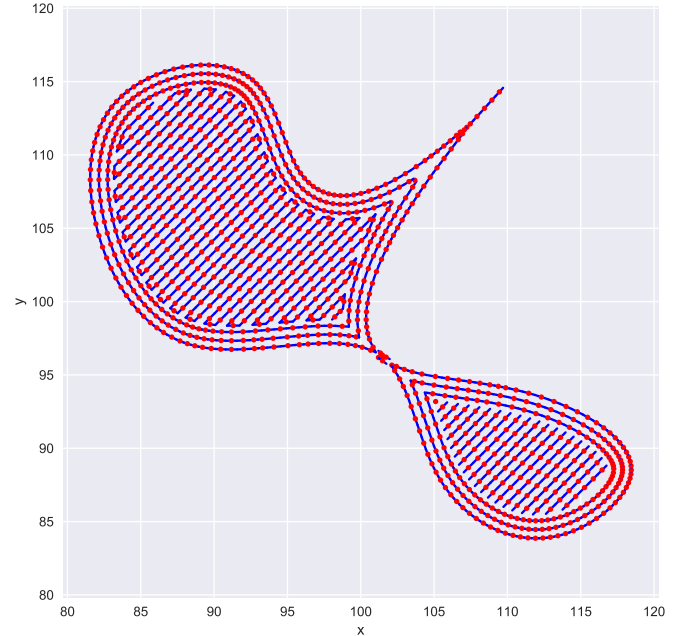


FIGURE 2: Discretization example

the latter model also predicting densification. Hodge et al. [18] applied a 3D-coupled, thermal-mechanical FE model to conduct part-scale simulations and to investigate optimal conditions for manufacturing overhanging sections.

Antony et al. [19] used finite element and experimental analysis to study the PBF melting process of 316L stainless-steel powders. The authors investigated the effects of wetting angles and balling (when the melt pool tends to ball up rather than forming one continuous track if the length to width ratio of the track is too high). Simchi et al. [11] used empirical data to determine the relationships between energy input and densification in PBF. Nelson et al. [20] used empirical data to create a 1D heat transfer model able to predict melting depths.

Gusarov et al. [9, 21–23] have modeled radiation transfer in powder bed fusion. Researchers in Zaeh research group at Technical University of Munich have published several papers on part level modeling of both laser and electron beam melting, including the modeling of complete part fabrication [24–32]. Lawrence Livermore National Laboratory [33–35] proposed a multi-scale modeling strategy of PBF that includes a powder-scale model which simulates single track builds. These models provide powder bed and melt pool thermal data, while an additional model computationally builds a complete part and predicts manufactured properties. Yan et al [36] proposed a high-fidelity powder-scale model to predict the defect mechanisms in electron beam melting.

Zohdi et al at the University of California at Berkeley has applied the discrete element method (DEM) to study the melting

process [37–41] of selective laser sintering (SLS). In their simulations, the material was treated as discrete particles instead of a continuum medium. The thermal transfer is modeled through conduction between particles and the thermal interactions between the laser beam and particles. Michopoulos et al at the Naval Research Laboratory has developed an approach called the multi-physics discrete element method (MDEM) to simulate powder-based AM by extending the DEM beyond Newtonian mechanics. These extensions include the multiple physics of capturing granular dynamics, energy application and conservation [42–45]. The same group also developed a semi-analytic method which is called enriched analytic solution methodology (EASM) [46]. This method is used to model the thermal aspect of AM through extending analytic solutions of linear heat equation to non-linear heat equation and it achieves high computational efficiency.

Overall, there appears to be two main issues with the current research. First, reduced-order models with simplified analytic solutions cannot be accurately applied to PBF processes. Second, continuous and powder-based simulations tend to be too computationally expensive to model realistic PBF processes and parts.

3 Formulation

To address these issues, we developed a path-level thermal model to simulate a PBF process for a single laser scan. The modeling approach involves two steps: (1) discretizing the scan path into path elements; (2) simulating the temperature evolution of the elements after a single scan of a laser beam. In the simulation, the temperature of each element is assumed to be uniform throughout the element due to its low *Biot* number [47].

3.1 Numerical scheme

The standard approach for formulating a transient thermal problem is based on the conservation of energy, which states that the energy variation in a volume over a given time period is equal to the difference between the heat produced in the volume and the net out-flowing heat. The integral governing equation of heat conservation of PBF process is written as

$$\int_{\omega} \rho c \dot{T} dV = \int_{\partial\omega} \mathbf{Q} \cdot \mathbf{n} dA + \int_{\omega} H dV, \quad (1)$$

where ω represents the domain of interest, ρ is density, c is the constant pressure specific heat capacity of the material, T is temperature, \mathbf{Q} denotes the thermal flux on the domain's boundary, \mathbf{n} is the normal vector of dA , and H is the source term which accounts for energy input of laser scan.

The proposed simulation operates on the path level instead of the powder level. In the simulation the computation domain

(i.e., evolving melted volume) is discretized according to the scan path. Conceptually, the proposed simulation consists of two stages: pre-processing and execution. During the pre-processing stage, the scan path and laser power information are extracted from the manufacturing input file (e.g., G-code file), then the scan path is discretized into many short line segments (using the approach developed in [48, 49]).

Each path segment represents an element, called the path element. The path element approximates the newly melted volume generated by the laser scan on the corresponding segment in a short period of time. The deposition and growing of path elements during the simulation simulate the laser scan and powder melting during the manufacturing process. The real solution of Eqn. 1 could satisfy conservation of energy laws in arbitrary temporal and spatial conditions. We approximate the real solution by enforcing the conservation of energy on a discretization of space (i.e., element) and time.

Since the size of a path element is very small (due to its short length and thin layer height), its *Biot* number is low, which means the path element is “thermally simple” and the interior of the element maybe presumed to be a uniform temperature. A lumped-capacitance model is used to conduct the thermal simulation, so the temperature distribution is assumed uniform throughout each path element. The evolving fabrication domain is discretized into many path elements according to the laser path plan. Subsequently, the heat conservation equation for the *i*-th element can be obtained.

$$m_i c_i \dot{T}_i = Q_i + H_i, \quad (2)$$

where m is the mass of the *i*-th element, Q_i denotes the heat transfer term, and H_i represents the term that accounts for the energy absorbed from the laser scan. The heat transfer on element boundary can be divided into several thermal effects: conduction, convection, and radiation. Next, we elaborate on each of the types of thermal effects in detail.

$$Q_i = Q_i^{cond} + Q_i^{conv} + Q_i^{rad}, \quad (3)$$

where Q^{cond} , Q^{conv} , Q^{rad} represent conductive, convective and radiative term respectively. The conductive term in the above equation includes: 1) conduction to neighboring elements along the scan path; 2) conduction to the powder bed; and 3) conduction to the substrate. In this paper, only single laser scan is considered, so there is no heat conduction to adjacent path elements. The formula for the conduction term is written as

$$Q_i^{cond} = \lambda \left(A_{i,i-1} \frac{T_i - T_{i-1}}{L_i + L_{i-1}} + A_{i,i+1} \frac{T_i - T_{i+1}}{L_i + L_{i+1}} \right) + A_i^{side} h_c^p (T_i - T_p) + A_i^{bottom} h_c^s (T_i - T_s), \quad (4)$$

where λ is the thermal conductivity; T_i is the temperature of i -th path element; $A_{i,j}$ is the cross-sectional area between path elements i and j ; L_i is the length of the i -th path element. A_i^{side} and A_i^{bottom} are the side area and bottom area of the element respectively, where A_i^{side} is the contact area between the element and powder bed (which includes two sides) and A_i^{bottom} is the contact area between the element and substrate; T_p and T_s are the temperatures of powder bed and substrate (which are assumed to be constant in the simulation); h_c^p is the thermal contact conductance between the path element and powder bed; And h_c^s is the thermal contact conductance between the path element and substrate.

Assuming the ambient temperature is T_{env} , the convection term can be written as

$$Q_i^{conv} = h_{conv}(T_i - T_{env})A_i^{free}, \quad (5)$$

where h_{conv} is the convective heat transfer coefficient and A_i^{free} is the free surface area facing the ambient environment. The radiation term can be expressed as

$$Q_i^{rad} = \varepsilon \sigma_{SB}(T_i^4 - T_{env}^4)A_i^{free}, \quad (6)$$

where ε is the material emissivity and σ_{SB} is the *Stefan-Boltzmann* constant ($\sigma_{SB} = 5.67 \times 10^{-8} \text{ W/m}^2 \text{ K}^4$) [47]. Note that convective and radiative heat transfer are considered only on the top surface of the path element. The Kelvin scale should be used when calculating radiation.

3.2 Laser modeling

To compute the laser term H , we need to model the laser scan and laser energy absorption. In powder-level simulations (such as discrete element method) each element is modeled as a single spherical particle, therefore laser absorption can be modeled in a relatively simple manner. However, the proposed simulation is based on path level, each element is composed of multiple powder particles, complicating the interactions between the powder and laser. The laser heating term $H(x, y)$ for an infinitesimal (centered at (x, y)) is given as

$$H(x, y) = \alpha I(r, z) dxdy, \quad (7)$$

where α is the absorptivity of the material at the wavelength of the laser ($0 \leq \alpha \leq 1$) [4]; $I(r, z)$ denotes the laser intensity (W/m^2) which is the function of the radial distance (r) between the laser beam center and (x, y) and the penetration depth z . And $dxdy$ is the projected area of the infinitesimal receiving direct, normal radiation from the laser. In order to compute the laser heating term for a path element, we need to integrate $H(x, y)$ on the top surface of the path element.

It is common to assume the laser beam used in PBF process is Gaussian, which means the laser intensity decreases exponentially as the radial distance from laser beam's center increases. Also a Beer-Lambert type model is used for laser penetration, where laser intensity decreases exponentially with respect to the penetration depth [4]. Then laser intensity could be expressed as:

$$I(r, z) = I_0 e^{-\beta z} e^{-2r^2/\omega^2}, \quad (8)$$

where $I_0 = \frac{2 \times P}{\pi \omega^2}$ is the peak intensity; P is the laser power; ω is the beam spot size measured to where the intensity falls to $1/e^2$ of the peak intensity; And β is the optical extinction coefficient. The theory in [21, 23] is used to compute optical extinction coefficient (β) which is a function of particle diameter, D and powder bed porosity, γ .

$$\beta = \frac{3(1 - \gamma)}{2\gamma D} \quad (9)$$

The metal powders are treated as sphere particles. And diameter distribution is modeled as a truncated Gaussian distribution. For example, the mean diameter, μ_D , can be given as $30 \mu\text{m}$ and the diameter as $D \in [10 \mu\text{m}, 50 \mu\text{m}]$. In our simulation the mean diameter is used to estimate the average optical extinction coefficient β_{avg} for the path element.

$$\beta_{avg} = \frac{3(1 - \gamma)}{2\gamma \mu_D} \quad (10)$$

The top surface of the element is not assumed to be perfectly flat due to the fact that element is composed of powder particles, which means the penetration depth z is not zero. The mean absolute deviation (around the mean) of the powder diameter is used to estimate the average penetration depth z_{avg} from the laser beam center. For a normal distribution random variable X , with mean 0 and variance σ^2 (i.e., $X \sim N(0, \sigma^2)$), the ratio of mean absolute deviation to standard deviation is $\sqrt{2/\pi}$. In other words, the mean absolute deviation is about 0.8 times the standard deviation. The estimated average penetration depth z of the path element can now be computed as

$$z_{avg} = \sigma_D \sqrt{\frac{2}{\pi}} \quad (11)$$

Assuming center of laser beam is located at (x_0, y_0) , substitute the formulas of β_{avg} and z_{avg} into Equation (8) and integrate term $H(x, y)$ on the top surface of the element (defined as an axis

aligned rectangle $[x_1, x_2] \times [y_1, y_2]$, laser heating term H for element is obtained.

$$H = \alpha \frac{2P}{\pi\omega^2} e^{-\beta_{avg}z_{avg}} \times \frac{1}{8} \pi\omega^2 \times W \quad (12)$$

$$= \frac{1}{4} \alpha e^{-\beta_{avg}z_{avg}} P \cdot W$$

where $W = (f(x_0, x_2) - f(x_0, x_1)) \times (f(y_0, y_2) - f(y_0, y_1))$ and $f(a, b) = erf(\frac{\sqrt{2}(a-b)}{\omega})$, $erf(\cdot)$ is the error function. Equation (12) is the formula for the laser heating term H for an axis aligned path element. From it, we can see H is proportional to laser power P and material absorptivity α . The main work during computing H is in computing W . The value of W is determined by the relative position of the laser beam center and the path element.

3.3 Material properties

Temperature deviations in PBF process are much larger than those typically associated with polymer processes, as metal powder is melted or even evaporated during the manufacturing process. Therefore, assumptions made about fixed material properties in our work with polymer processes are no longer valid. Additionally, according to numerical experiments, material properties have a huge impact on computed results. Therefore, material properties are functions of temperature in the proposed simulation.

Using 316L stainless steel (316L SS) as an example, the specific heat, thermal conductivity and density values are given as a function of temperature and phase in Table 1 [4]. In the proposed simulation, the same technique in the literature is applied, where properties are linearly interpolated at temperature values in between specified data points. Also, the data is extrapolated up to 1400 K (the final measured values are at 1255 K), after which the property values are fixed until phase change occurs at 1700 K.

TABLE 1: Material properties for 316L stainless steel as a function of temperature [4]

Temperature (K)	Specific heat (J/kg K)	Thermal conductivity (W/mK)	Density (kg/m ³)
293	452	13.3	7952
366	485	14.3	7919
478	527	15.9	7877
589	548	17.5	7831
700	565	19.0	7786
811	573	19.8	7739
922	586	21.9	7692
1033	615	23.2	7640
1144	649	24.6	7587
1255	690	26.2	7537
1700 (liquid)	815	32.4	7300

Due to the latent heat, specific heat capacity is more difficult to determine than thermal conductivity or density. Latent heat is thermal energy released or absorbed, usually at a phase change, during a constant-temperature process. To account for the latent heat, we adopt an apparent heat capacity method similar to those outlined by Bonocina et al. [50] and, more recently, by Muhieddine et al. [51]. In this method, the energy needed for a phase change to occur is considered by computationally raising the specific heat of the material in a small range (ΔT) around the melting or vaporization temperatures. Specific heat capacity is represented by a staircase function. The formula for heat capacity c is outlined as follows:

$$c = \begin{cases} c_{solid}, & T < T_m - \frac{\Delta T}{2} \\ \frac{c_{solid} + c_{liquid}}{2} + \frac{L_{m/s}}{\Delta T}, & T_m - \frac{\Delta T}{2} \leq T \leq T_m + \frac{\Delta T}{2} \\ c_{liquid}, & T_m + \frac{\Delta T}{2} < T < T_v - \frac{\Delta T}{2} \\ \frac{c_{liquid} + c_{gas}}{2} + \frac{L_{v/c}}{\Delta T}, & T_v - \frac{\Delta T}{2} \leq T \leq T_v + \frac{\Delta T}{2} \\ c_{gas}, & T > T_v + \frac{\Delta T}{2} \end{cases} \quad (13)$$

where T_m is the melting temperature; T_v is the vaporization (or boiling) temperature; $L_{m/s}$ is the latent heat from melting or solidification, and $L_{v/c}$ is the latent heat from vaporization or condensation.

With the above formula, we can plot the capacity curve shown in Figure 3. For clarity, this figure does not address the vaporization point. Essentially, capacity jumps when a temperature is around the phase change temperature, which takes the latent heat into account.

3.4 Element growth mechanism

The proposed thermal simulation is based on the composition of discussed manufacturing primitives (i.e., laser scan), and the domain is composed of a sequence of n elements. All elements on a continuous laser scan, except for the first and last elements, contact their predecessors and successors at their cross sections. The initial (final) cross section of the first (last) element is treated as a free boundary. For PBF, a path element is formed by the heat transfer process initiated by melting the metal powder with a laser scan. In this case, formulating and solving the associated heat-transfer equation is difficult because of the co-dependent relationship: the heat associated with a path element influences the heat transfer, while the shape of path element is determined by the heat transfer process. This co-dependency exists due to the nature of our simulation, which tries to approximate the process without simulating the whole powder bed.

Recall, that each element is defined by the newest melted material. Consequently, we attack the co-dependency problem by introducing an element-growth mechanism. Here element growth refers specifically to the width of that melted material. This means that the elements width has a dynamic value in the

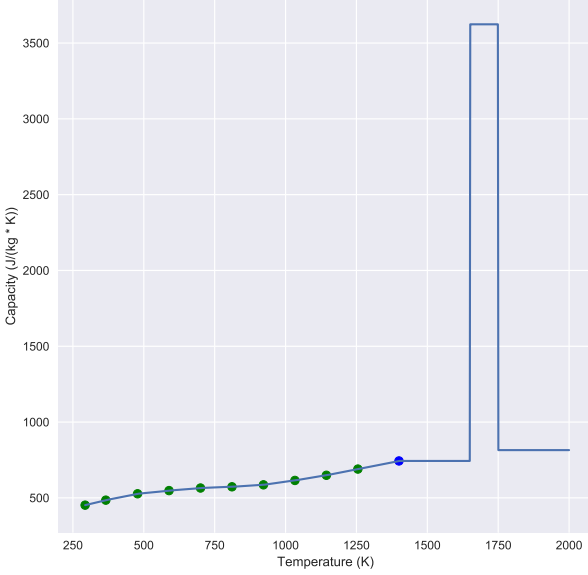


FIGURE 3: Specific heat capacity of 316L stainless steel.

simulation, which mimics the actual melting process. Each element is initialized with an initial width that typically is determined by empirical data or high-fidelity, numerical simulations. We set an element's initial width to be the laser spot size, which relates to where the material will absorb the most laser energy. Since there is no element shrinking mechanism in the simulation, the initial element width is intended to be less than the final width again, this corresponds to reality. In each time step during the simulation, an element's width will grow according to its thermal conditions. Essentially, this is an iterative correction procedure. For a single laser scan, the final element width will equal the width of the melt pool as it passes completely through an element.

To describe the element growth mechanism, we address two questions. First, at what time in the simulation should an element grow its width? An element grows when it absorbs heat and a phase change begins; so, it is reasonable to trigger the width growth when an element's temperature is higher than some preset threshold. Since the apparent heat capacity method is used in the simulation, the threshold is set to be $T_m + \frac{\Delta T}{2}$ (T_m is melting temperature). This means that, during the simulation, whenever an element's temperature is greater than $T_m + \frac{\Delta T}{2}$ the element will expand its width during that time step.

Second, when the element does grow, how much should it grow? The simulation calculates the growth quantity based on energy conservation. For single laser scan, the element grows

symmetrically with respect to its center line. The energy transferred from the melted element to the powder bed in this time step is used in updating element's width.

$$A_i^{side} h_c^p (T_i - T_p) \cdot \Delta t = 0.5 \cdot A_i^{side} W_{grow} \rho_p c_{avg} (T_i - T_p) \quad (14)$$

where W_{grow} is the width growth quantity; ρ_p is the powder density; T_i is the temperature of the element; T_p is the temperature of the powder bed; and c_{avg} is the average capacity of the powder, which is computed by integrating the capacity curve.

3.5 Simulation

There are two stages in our simulation: the pre-process stage and the execution stage. During the pre-process stage, the laser path is discretized into path elements. Each element keeps track of its own length, width, height, state, and temperature. The state variable denotes the current state of the element. At the start of the simulation, we set the initial state of all the elements to "powder". As the simulation progresses, an element is heated until it reaches its melting temperature, when its state changes to liquid. Then the element cools until its temperature is below the melting temperature, when its state changes to solid. Since the current simulation only involves a single laser track, initially all elements are active.

In execution stage, a standard Forward Euler (FE) time-marching scheme is used to update the temperature of each element.

$$T_i(t + \Delta t) \approx T_i(t) + \Delta t \cdot \dot{T}_i(t) \quad (15)$$

where $\dot{T}_i(t)$ can be computed using Equation 2. Basically each time step involves three steps:

1. Update the center position of the laser beam according to the path plan
2. For each element:

Compute the total thermal power for each of the thermal effects, including: the laser heating term (H), convection, radiation, heat conduction along the path, heat conductance to the build platform, and heat conductance to the powder bed.

Compute the temperature change at this time step.

3. Update the temperatures and element states of all elements. When conditions are satisfied, grow the width of the element according to the mechanism described in Section 3.4.

The output of the simulation is the complete temperature history of each path element over the course of a fabrication. We can compute a melt pool's position, shape, size through the course of a manufacturing process based on that history. When

the simulation ends, the solidified geometry can be determined by combining the final positions and sizes of all elements.

4 Validation and tests

To validate the proposed simulation, we conducted two numerical experiments. In the first experiment, the melt pool width predictions from our model were compared against actual melt pool widths in [34] and numerical results from Zohdi et al [4]. These comparisons were made for a single pass of a Gaussian laser over a single layer of powder particles resting on a substrate. In the second experiment, we compared our results from simulating a single straight laser scan of PBF process against experimental and high-fidelity numerical results published by NIST.

In the first experiment, we used the same experimental settings (material properties, laser parameters, domain size, etc.) and data (Figure 4) as those described in the literature [34]. Khairallah and Anderson observed an experimental melt pool width of $75 \mu\text{m}$, while their simulation predicted a melt pool width of $72 \mu\text{m}$. The melt pool width obtained by our meso-scale simulation is $78 \mu\text{m}$. For comparison, the coupled DE-FD approach described in [4] predicts a melt pool width $85 \mu\text{m}$. Melt pool predictions from our simulation compare well with the experiment and simulation results of others.

In support of our claim of reduced computational costs, our proposed meso-scale simulation only required about 10 CPU seconds to run. In comparison, the coupled DE-FD framework takes several CPU hours to run and the ALE framework used in the simulations from [34] requires on the order of 100,000 CPU hours. Thus, in our view, the meso-scale simulator has the capability to be used as a quick tool to predict melt pool size. This capability allows for the quick optimization of process parameters for different materials and/or powder size distributions.

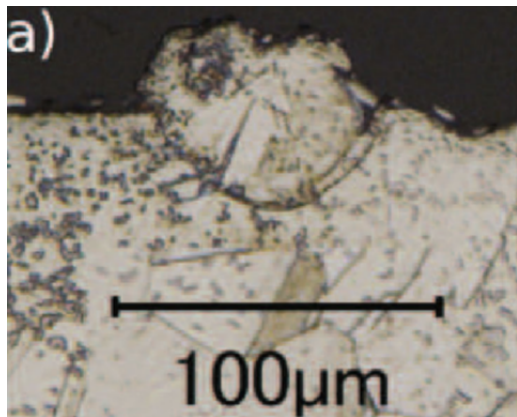


FIGURE 4: Experimental micrograph conducted by Khairallah and Anderson [34].

In the second experiment, we used the proposed simulation to predict the melt pool width of a single, straight, laser scan of the L-PBF process using Inconel Alloy 625 (IN625). The predicted melt pool width was compared against experimental results as well as the numerical results obtained from high fidelity simulations conducted by NIST. The comparison is listed in the table below (Table 2). In each record, the first column shows NIST’s high fidelity result, the second column contains NIST’s experimental data (NA means not available), and our simulation result is in the last column. There are three levels of laser speed and two levels of laser power shown in the table. In order to measure the accuracy of the proposed simulation, the mean absolute percentage error (MAPE) is computed. The MAPE of the simulation results with respect to NIST’s experimental data is 5.9 %. The MAPE of the simulation results with respect to NIST’s high fidelity result is 4.6 %. Therefore the results obtained from the proposed simulation agree well with the results from NIST.

Based on the comparisons discussed in this section, we believe that the element growth mechanism, which is the heart of our simulation, can capture the elements width very well. We believe that those favorable comparisons validate our meso-scale, thermal-simulation approach.

TABLE 2: Comparison of melt pool width results

	195 W	122 W
0.2 m/s	248/227/238 μm	184/158/177 μm
0.5 m/s	160/150/164 μm	135/127/129 μm
0.8 m/s	127/132/134 μm	113/NA/105 μm

5 Conclusion and future directions

5.1 Summary and significance

The main contribution of the paper is using a path-level thermal simulation to model the melt pool evolution during a powder bed fusion process. The proposed simulation has three novel ingredients. First, our simulation is formulated directly from manufactured geometry while incorporating the essential physics during the manufacturing process. These physics include laser energy absorption, thermal convection and radiation to an ambient environment, metal power melting and evaporation, and the thermal interactions among the melt pool, the powder bed, and the underneath substrate. Second, the simulation model discretizes a scan path into path elements and uses an explicit method to calculate thermal history, which does not require solving a system of linear equations at each time step. Finally, the

model simulates the evolution of the melt pool at the meso-scale by introducing an element growth mechanism. The combination of these three ingredients makes our thermal simulation more efficient than both a powder-based simulation (e.g., DEM) and a voxelization-based simulation (e.g., FEM). The simulation has been validated against both experimental data and simulation results from the literature and NIST, however, additional validation will be needed in application.

5.2 Extensions and Promising Directions

The current simulation models a single laser scan only. We plan to extend the models to accommodate process plans for the fabrication of more complicated 3D shapes. We believe that the efficiency of the current model makes this possible. In addition, we believe that many of the concepts we used to model PBF processes can be extended to other AM processes that are driven by a moving heat source. Finally, the ability to efficiently predict the melt pool size during the PBF process opens many possibilities for solving the inverse problem of optimizing manufacturing parameters for a given geometry and building feedback-control mechanisms to guide against failures during the manufacturing process.

ACKNOWLEDGMENT

This research is supported by NSF grants CMMI-1344205 and CMMI-1361862 and the National Institute of Standards and Technology. The responsibility for errors and omissions lies solely with the authors.

DISCLAIMER

Certain commercial equipment, instruments, or materials (or suppliers, or software, ...) are identified in this paper to foster understanding. Such identification does not imply recommendation or endorsement by the National Institute of Standards and Technology, nor does it imply that the materials or equipment identified are necessarily the best available for the purpose.

REFERENCES

- [1] Sames, W. J., List, F., Pannala, S., Dehoff, R. R., and Babu, S. S., 2016. "The metallurgy and processing science of metal additive manufacturing". *International Materials Reviews*, **61**(5), pp. 315–360.
- [2] Bikas, H., Stavropoulos, P., and Chryssolouris, G., 2016. "Additive manufacturing methods and modelling approaches: a critical review". *The International Journal of Advanced Manufacturing Technology*, **83**(1-4), pp. 389–405.
- [3] Rodgers, T. M., Madison, J. D., and Tikare, V., 2017. "Simulation of metal additive manufacturing microstructures using kinetic monte carlo". *Computational Materials Science*, **135**, pp. 78–89.
- [4] Ganeriwala, R., and Zohdi, T. I., 2016. "A coupled discrete element-finite difference model of selective laser sintering". *Granular Matter*, **18**(2), p. 21.
- [5] Zeng, K., Pal, D., and Stucker, B., 2012. "A review of thermal analysis methods in laser sintering and selective laser melting". In *Proceedings of Solid Freeform Fabrication Symposium Austin, TX*, pp. 796–814.
- [6] Kruth, J.-P., Froyen, L., Van Vaerenbergh, J., Mercelis, P., Rombouts, M., and Lauwers, B., 2004. "Selective laser melting of iron-based powder". *Journal of materials processing technology*, **149**(1-3), pp. 616–622.
- [7] Yadroitsev, I., Bertrand, P., and Smurov, I., 2007. "Parametric analysis of the selective laser melting process". *Applied surface science*, **253**(19), pp. 8064–8069.
- [8] McCarthy, B., 2015. "Characterization of geometric deviations in FDM". Master's thesis, University of Wisconsin-Madison, United States.
- [9] Tolochko, N. K., Arshinov, M. K., Gusarov, A. V., Titov, V. I., Laoui, T., and Froyen, L., 2003. "Mechanisms of selective laser sintering and heat transfer in ti powder". *Rapid prototyping journal*, **9**(5), pp. 314–326.
- [10] Wang, X., Laoui, T., Bonse, J., Kruth, J.-P., Lauwers, B., and Froyen, L., 2002. "Direct selective laser sintering of hard metal powders: experimental study and simulation". *The International Journal of Advanced Manufacturing Technology*, **19**(5), pp. 351–357.
- [11] Simchi, A., 2006. "Direct laser sintering of metal powders: Mechanism, kinetics and microstructural features". *Materials Science and Engineering: A*, **428**(1-2), pp. 148–158.
- [12] Carslaw, H., and Jaeger, J., 1959. *Conduction of heat in solids: Oxford Science Publications*. Oxford, England.
- [13] Dai, K., Li, X., and Shaw, L., 2004. "Comparisons between thermal modeling and experiments: effects of substrate preheating". *Rapid Prototyping Journal*, **10**(1), pp. 24–34.
- [14] Dai, K., and Shaw, L., 2004. "Thermal and mechanical finite element modeling of laser forming from metal and ceramic powders". *Acta Materialia*, **52**(1), pp. 69–80.
- [15] Matsumoto, M., Shiomi, M., Osakada, K., and Abe, F., 2002. "Finite element analysis of single layer forming on metallic powder bed in rapid prototyping by selective laser processing". *International Journal of Machine Tools and Manufacture*, **42**(1), pp. 61–67.
- [16] Dong, L., Makradi, A., Ahzi, S., and Remond, Y., 2009. "Three-dimensional transient finite element analysis of the selective laser sintering process". *Journal of materials processing technology*, **209**(2), pp. 700–706.
- [17] Kolossov, S., Boillat, E., Glardon, R., Fischer, P., and Locher, M., 2004. "3d fe simulation for temperature evo-

- lution in the selective laser sintering process”. *International Journal of Machine Tools and Manufacture*, **44**(2-3), pp. 117–123.
- [18] Hodge, N., Ferencz, R., and Solberg, J., 2014. “Implementation of a thermomechanical model for the simulation of selective laser melting”. *Computational Mechanics*, **54**(1), pp. 33–51.
- [19] Antony, K., Arivazhagan, N., and Senthilkumaran, K., 2014. “Numerical and experimental investigations on laser melting of stainless steel 316l metal powders”. *Journal of Manufacturing Processes*, **16**(3), pp. 345–355.
- [20] Nelson, J. C., Xue, S., Barlow, J. W., Beaman, J. J., Marcus, H. L., and Bourell, D. L., 1993. “Model of the selective laser sintering of bisphenol-a polycarbonate”. *Industrial & Engineering Chemistry Research*, **32**(10), pp. 2305–2317.
- [21] Gusarov, A., Yadroitsev, I., Bertrand, P., and Smurov, I., 2009. “Model of radiation and heat transfer in laser-powder interaction zone at selective laser melting”. *Journal of heat transfer*, **131**(7), p. 072101.
- [22] Gusarov, A., and Smurov, I., 2010. “Modeling the interaction of laser radiation with powder bed at selective laser melting”. *Physics Procedia*, **5**, pp. 381–394.
- [23] Gusarov, A., and Kruth, J.-P., 2005. “Modelling of radiation transfer in metallic powders at laser treatment”. *International Journal of Heat and Mass Transfer*, **48**(16), pp. 3423–3434.
- [24] Krol, T. A., Westhäuser, S., Zäh, M. F., and Groth, C., 2010. “Dynamic coupling of fe-models for additive manufacturing to regard the customer requirements”. In Proceedings of the ANSYS Conference and 28. CADFEM Users Meeting 2010, Vol. 12, pp. 169–174.
- [25] Zaeh, M., and Ott, M., 2011. “Investigations on heat regulation of additive manufacturing processes for metal structures”. *CIRP Annals-Manufacturing Technology*, **60**(1), pp. 259–262.
- [26] Zaeh, M. F., and Branner, G., 2010. “Investigations on residual stresses and deformations in selective laser melting”. *Production Engineering*, **4**(1), pp. 35–45.
- [27] Krol, T., Zaeh, M., and Seidel, C., 2012. “Optimization of supports in metal-based additive manufacturing by means of finite element models”. In Solid Freeform Fabrication Symposium, Austin, TX, pp. 707–718.
- [28] Krol, T., Seidel, C., and Zaeh, M., 2013. “Prioritization of process parameters for an efficient optimisation of additive manufacturing by means of a finite element method”. *Procedia CIRP*, **12**, pp. 169–174.
- [29] Zaeh, M., Branner, G., and Krol, T., 2009. “A three dimensional fe-model for the investigation of transient physical effects in selective laser melting”. In *Innovative Developments in Design and Manufacturing*. CRC Press, pp. 433–442.
- [30] Krol, T., Seidel, C., Schilp, J., Hofmann, M., Gan, W., and Zaeh, M., 2013. “Verification of structural simulation results of metal-based additive manufacturing by means of neutron diffraction”. *Physics Procedia*, **41**, pp. 849–857.
- [31] Zäh, M. F., and Lutzmann, S., 2010. “Modelling and simulation of electron beam melting”. *Production Engineering*, **4**(1), pp. 15–23.
- [32] Eschey, C., Lutzmann, S., and Zaeh, M., 2009. “Examination of the powder spreading effect in electron beam melting (ebm)”. *Solid Freeform Fabrication, Austin, TX, August*, pp. 3–5.
- [33] Vasudevarao, B., Natarajan, D. P., Henderson, M., and Razdan, A., 2000. “Sensitivity of rp surface finish to process parameter variation”. In Solid freeform fabrication proceedings, The University of Texas Austin, pp. 251–258.
- [34] Khairallah, S. A., and Anderson, A., 2014. “Mesoscopic simulation model of selective laser melting of stainless steel powder”. *Journal of Materials Processing Technology*, **214**(11), pp. 2627–2636.
- [35] King, W., Anderson, A., Ferencz, R., Hodge, N., Kamath, C., and Khairallah, S., 2015. “Overview of modelling and simulation of metal powder bed fusion process at lawrence livermore national laboratory”. *Materials Science and Technology*, **31**(8), pp. 957–968.
- [36] Yan, W., Ge, W., Qian, Y., Lin, S., Zhou, B., Liu, W. K., Lin, F., and Wagner, G. J., 2017. “Multi-physics modeling of single/multiple-track defect mechanisms in electron beam selective melting”. *Acta Materialia*, **134**, pp. 324–333.
- [37] Zohdi, T., 2014. “Additive particle deposition and selective laser processing-a computational manufacturing framework”. *Computational Mechanics*, **54**(1), pp. 171–191.
- [38] Zohdi, T., 2014. “A direct particle-based computational framework for electrically enhanced thermo-mechanical sintering of powdered materials”. *Mathematics and Mechanics of Solids*, **19**(1), pp. 93–113.
- [39] Zohdi, T. I., 2013. “Rapid simulation of laser processing of discrete particulate materials”. *Archives of Computational Methods in Engineering*, **20**(4), pp. 309–325.
- [40] Zohdi, T., 2012. “Estimation of electrical heating load-shares for sintering of powder mixtures”. *Proc. R. Soc. A*, **468**(2144), pp. 2174–2190.
- [41] Ganeriwala, R., and Zohdi, T. I., 2014. “Multiphysics modeling and simulation of selective laser sintering manufacturing processes”. *Procedia CIRP*, **14**, pp. 299–304.
- [42] Steuben, J. C., Iliopoulos, A. P., and Michopoulos, J. G., 2016. “Discrete element modeling of particle-based additive manufacturing processes”. *Computer Methods in Applied Mechanics and Engineering*, **305**, pp. 537–561.
- [43] Steuben, J. C., Iliopoulos, A. P., and Michopoulos, J. G., 2016. “On multiphysics discrete element modeling of powder-based additive manufacturing processes”. In ASME 2016 International Design Engineering Technical

- Conferences and Computers and Information in Engineering Conference, American Society of Mechanical Engineers, pp. V01AT02A032–V01AT02A032.
- [44] Steuben, J. C., Iliopoulos, A. P., and Michopoulos, J. G., 2017. “Recent developments of the multiphysics discrete element method for additive manufacturing modeling and simulation”. In ASME 2017 International Design Engineering Technical Conferences and Computers and Information in Engineering Conference, American Society of Mechanical Engineers, pp. V001T02A025–V001T02A025.
- [45] Michopoulos, J. G., Iliopoulos, A. P., Steuben, J. C., Birnbaum, A. J., and Lambrakos, S. G., 2018. “On the multiphysics modeling challenges for metal additive manufacturing processes”. *Additive Manufacturing*, **22**, pp. 784–799.
- [46] Steuben, J. C., Birnbaum, A. J., Michopoulos, J. G., and Iliopoulos, A. P., 2019. “Enriched analytical solutions for additive manufacturing modeling and simulation”. *Additive Manufacturing*, **25**, pp. 437–447.
- [47] Bergman, T. L., Incropera, F. P., DeWitt, D. P., and Lavine, A. S., 2011. *Fundamentals of heat and mass transfer*. John Wiley & Sons.
- [48] Zhang, Y., and Shapiro, V., 2017. “Linear time thermal simulation of fdm process”. In ASME 2017 International Design Engineering Technical Conferences and Computers and Information in Engineering Conference, American Society of Mechanical Engineers, pp. V001T02A033–V001T02A033.
- [49] Zhang, Y., and Shapiro, V., 2018. “Linear-time thermal simulation of as-manufactured fused deposition modeling components”. *Journal of Manufacturing Science and Engineering*, **140**(7), p. 071002.
- [50] Bonacina, C., Comini, G., Fasano, A., and Primicerio, M. ., 1973. “Numerical solution of phase-change problems”. *International Journal of Heat and Mass Transfer*, **16**(10), pp. 1825–1832.
- [51] Muhieddine, M., Canot, E., and March, R., 2009. “Various approaches for solving problems in heat conduction with phase change”. *International Journal on Finite Volumes*, p. 19.